# Photoinduced electron transfer in semiconductor clay binary nanosheet colloids controlled by clay particles as a turnout switch


doi: https://doi.org/10.1016/j.apcatb.2018.09.047

# Photoinduced electron transfer in semiconductor–clay binary nanosheet colloids controlled by clay particles as a turnout switch

Teruyuki Nakato,[a,b,*] Shinya Terada,[a] Tatsuya Ishiku,[a] Shungo Abe,[a] Sunao Kamimura,[a] Emiko Mouri,[a,b] and Teruhisa Ohno[a,b]

[a] Department of Applied Chemistry, Kyushu Institute of Technology

[b] Strategic Research Unit for Innovative Multiscale Materials, Kyushu Institute of Technology

1-1 Sensui-cho, Tobata-ku, Kitakyushu, Fukuoka 804-8550, Japan

*nakato@che.kyutech.ac.jp

**Abstract**

Although semiconductor photocatalysis has been investigated actively for a long time, control of dark processes successive to electron transfer from photocatalysts is almost unexplored compared with designing photocatalysts themselves. The present study proposes employment of clay particles as for controlling the dark processes independently of semiconductor photocatalyst particles. We employed niobate–clay binary nanosheet colloids, where colloidal niobate and clay nanosheets are spatially separated at a micrometer level. Niobate nanosheets worked as the semiconductor photocatalyst that released electrons upon UV excitation, and clay nanosheets worked as the turnout switch of the released electrons to determine their destination. When methylviologen ($MV^{2+}$) molecules that accept the electrons released from niobate were adsorbed on the clay nanosheets, reduction of $MV^{2+}$ predominantly occurred, and hydrogen was little evolved from the colloid. When Pt nanoparticles were deposited on clay nanosheets, photocatalytic hydrogen evolution occurred because Pt loaded on clay nanoparticles played a role of cocatalyst. When $MV^{2+}$ and Pt were co-loaded on clay nanosheets, both of the $MV^{2+}$ reduction and hydrogen evolution occurred competitively. The photocatalytic hydrogen evolution carried out by stirring the colloid sample was worse than that conducted without stirring, which indicated positive contribution of the spatial separation of photocatalytic niobate and cocatalytic clay nanosheets.

Keywords: Nanosheet colloid; Phase separation; Photocatalytic hydrogen evolution; Photoinduced electron transfer

## 1. Introduction

Heterogeneous photocatalytic and photochemical reactions are important in diverse fields such as energy conversion, environmental protection, and production of useful chemicals [1-3]. A variety of photocatalytic and photochemical reactions have been carried out in colloidal systems, where (photo)catalytic particles are dispersed in a reactant solution to provide heterogeneous reaction media. Such reactions in colloidal systems are enhanced by compositional and structural modification of particles themselves. For photocatalysis of semiconductor particles, a number of reaction systems have been developed in order to realize increased efficiency and selectivity. Meanwhile, many attempts have been proposed to overcome drawbacks of semiconductor photocatalysts represented by $TiO_2$ themselves, such as limited light absorption, efficient recombination, fast backward reaction, uncontrolled selectivity, and so forth [4].

A main strategy for developing colloidal photocatalytic systems has been precise design of photocatalytic particles themselves, as exemplified by doping or loading of cocatalysts, such as Pt, NiO, and $RuO_2$ [5, 6], and sensitizers, such as various organic dyes and plasmonic particles [7-9]. Diverse heterostructured multicomponent photocatalysts have been developed to promote various photocatalytic reactions for several decades [10, 11]. Such photocatalysts usually have complexed nanostructures where additional components such as cocatalysts and another photocatalytic species are precisely deposited on photocatalytic particles often through time-consuming complicated procedures.

However, simple mixing of plural particle species also improves the photocatalytic performance. A known example is synergetic effects of physical mixing of anatase and rutile particles on $TiO_2$ photocatalysis [12]. Metallic powders simply

dispersed together with photocatalysts can work as cocatalysts [13]. Z-scheme type photocatalytic reactions were initially carried out by simply adding two semiconductor photocatalysts into a reaction solution [14]. Assembly/dispersed structures of the colloidal particles also play important roles. $TiO_2$ nanoparticles aggregated into chain-like structures show enhancement of photocatalytic activities through efficient electron–hole separation facilitated by interparticle electron migration in the nanoparticle chains.[15, 16] Titanate nanodisks aggregated together with sensitizing quantum dots and cocatalyst particles show a higher photocatalytic activity than the isolated disks [17]. In these systems, particles coexisting with photocatalysts have certain photonic or electric functions such as light absorption and electron accumulation.

Photochemically inert and electrically insulating colloidal particles coexisting can also synergistically assist photocatalytic reactions of semiconductor oxides. Ide and coworkers have recently reported synergetic effects of photochemically inert layered silicates coexisting with $TiO_2$ photocatalyst [18-20]. Pure silicates, such as magadiite, and clay minerals, such as saponite and montmorillonite, exhibit such effects. They contribute to the photocatalytic reactions by precisely recognizing intermediates, products, or byproducts with their surfaces or interlayer spaces. As a result, the silicate particles alter the yield and selectivity of the reaction products in an unusual manner. Moreover, dyes intercalated into clay mineral particles can sensitize $TiO_2$ photocatalyst [21]. These pioneering studies suggest that we may develop various unusual photocatalytic systems by mixing modified silicate or clay particles, the modification which will enable the silicates to play other roles such as switching electron transfer directions.

In fact, we have recently reported synergistic effects of clay particles on

photocatalytic hydrogen evolution by semiconducting niobate particles [22]. In this system, both of the clay and niobate particles are heterocoagulated in a saline solution, and Pt cocatalyst is loaded not on the photocatalytic niobate particles but on the inert clay particles. Whereas photocatalytic properties of layered niobate $K_4Nb_6O_{17}$ crystallites have been well developed [23, 24], our results have clarified improvement of their photocatalytic activity by the clay particles coexisting in an appropriate manner. These findings prompt us to develop colloidal photocatalyst–clay systems where clay particles control dark reactions successive to the release of electrons from photoexcited photocatalytic particles. This is also inspired by natural photosynthetic systems, where dark reactions after photoinduced electron transfer from Photosystem I and II play important roles [25, 26]. If transfer of electrons released from semiconductor photocatalysts is regulated in the dark in the colloidal reaction system, we may approach precise control of photocatalytic reactions, although most of semiconductor photocatalyst researchers have paid attention to reaction control by regulating electron transfer processes between semiconductor photocatalysts and reactants.

Based on such motivation, we have designed a photocatalytic semiconductor–clay binary colloids where destination of electrons released from the semiconductor particles is determined by the clay particles. Reaction products are differentiated by appropriately modified clay particles independently of the photocatalyst, which means the role of turnout switch by modified clay particles. We employed colloidal nanosheets prepared by exfoliation of layered niobate $K_4Nb_6O_{17}$ and synthetic hectorite that is a smectite-type clay mineral [27]. Both of the layered compounds consist of anionic oxide layers and interlayer exchangeable cations, and are exfoliated in water to give nanosheets through infinite swelling of the interlayer spaces [28-30]. Niobate–clay

binary nanosheet colloid is characterized by phase separation of niobate and clay nanosheets at a micrometer scale; niobate and clay nanosheets are demixed and assembled into microdomains but apparently homogeneous at a macroscopic scale (Fig. 1) [31]. The demixing means spatial separation of two functional moieties, which are the photocatalytically active niobate and photochemically inert clay nanosheets. Another property of this binary colloid is selective adsorption of organic cations on clay nanosheets although both of the nanosheets are negatively charged [31, 32]. This property can be utilized to control interactions between the photocatalytic nanosheets and the organic species adsorbed on clay nanosheets [32-35]. In fact, if an electron acceptor is introduced to the colloid, photoinduced charge separation between the semiconducting niobate and the acceptor selectively adsorbed on clay is regulated by the clay content [32, 33].

The present study is a proof-of-concept trial of utilizing clay nanosheets in the niobate–clay binary system as a turnout switch that determines the destination of photogenerated electrons. Clay nanosheet surfaces were modified by electron acceptor molecules and/or Pt nanoparticles. While electron accepting methylviologen ($MV^{2+}$) [36] adsorbed on clay nanosheets accumulated electrons released by the niobate nanosheets, Pt nanoparticles on clay worked as a cocatalyst of hydrogen evolution by transferring electrons to aqueous $H^+$ ions. Coexistence of $MV^{2+}$ and Pt suppressed the electron accumulation in $MV^{2+}$ and electron transfer to $H^+$ by each other. Importance of spatial separation of clay nanosheets from photocatalytic niobate nanosheets at a microscopic scale was ensured by higher hydrogen evolution yield on irradiation under a static condition than that under a stirred condition. Although destination of electrons in photocatalytic reactions has been control by heterostructured photocatalysts, simple

mixing of turnout switch particles to the reaction system provides facile and adaptable ways for such purposes.

## 2. Experimental section

### *2.1. Instruments*

TEM images were obtained with a Hitachi H-90000NAR microscope. A small portion of a colloid sample was added to a mixture of water and methanol, and loaded on a grid coated with collodion membrane followed by drying at 313 K. X-ray photoelectron spectra (XPS) were recorded on a Kratos AXIS Nova spectrometer with a monochromatic Al Kα radiation. The binding energy was calibrated by taking the carbon (C) 1s peak of contaminant carbon as a reference at 284.6 eV. UV spectra were measured with a Shimadzu UV-2450 spectrophotometer by a transmission method.

### *2.2 Sample preparation*

Niobate nanosheets were prepared by exfoliation of tetrapotassium hexaniobate $K_4Nb_6O_{17}$ by the method reported previously [37, 38]. Single crystalline $K_4Nb_6O_{17}$ prepared from $K_2CO_3$ and $Nb_2O_5$ [39] was allowed to react with an aqueous solution of propylamine hydrochloride. The exfoliated material was recovered by centrifugation, washed, and dialyzed with water to yield the stock sample of niobate nanosheet LCs. Finally, the sample was dispersed in water to yield a stock colloid sample of niobate nanosheets. Laponite RD, synthetic hectorite clay (ideal formula $Na_{0.7}Si_8Mg_{5.4}Li_{0.4}H_4O_{24}$), was supplied by Rockwood Additives Ltd. Its cation exchange capacity (CEC) is 0.075 equivalents per 100 g clay [40]. As-received powdery clay sample was dispersed in water to yield a colloid of clay nanosheets.

Loading of $MV^{2+}$ onto clay nanosheets was carried out by slowly adding an aqueous solution of $MV^{2+}$ to clay colloid. Adsorption of $MV^{2+}$ on clay nanosheets was retained even after mixing with niobate nanosheets. Loading of Pt nanoparticles onto clay nanosheets was achieved by the clay-mediated in situ reduction reported by Varade and Haraguchi [41]. This method does not employ additional reducing agent for the Pt deposition, and ensures attachment of Pt nanoparticles on clay nanosheet surfaces. A clay colloid (10 g $L^{-1}$, 10 mL) was mixed with a 5wt% aqueous solution of $K_2PtCl_4$ and then heated at 333 K for 1 d in a capped vial. The amount of nominated Pt was 0.5wt% that of clay; all of the $PtCl_4^{2-}$ ions were assumed to be converted to metallic Pt. For comparison, we also prepared Pt-loaded niobate nanosheets, which will be indicated as Pt/niobate. Pt nanoparticles were deposited by loaded on niobate nanosheets through photodeposition by the method reported previously [22], and the amount of nominated Pt was 0.5wt% that of niobate.

Then, a small portion of the niobate colloid was mixed with a portion of a clay colloid and gently agitated to yield a niobate–clay binary nanosheet colloid sample. In order to distinguish the modification of clay nanosheets, we designate the clay nanosheets loaded by $MV^{2+}$, Pt, and both of $MV^{2+}$ and Pt as $MV^{2+}$/clay, Pt/clay, and $MV^{2+}$/Pt/clay, respectively; thus, the binary colloid is indicated as, for example, niobate–$MV^{2+}$/clay colloid. Composition of the standard samples was [niobate] = 1 g $L^{-1}$ and [clay] = 5 g $L^{-1}$; the niobate concentration [niobate] is given as the mass of $[Nb_6O_{17}]^{4-}$. $MV^{2+}$ was introduced to give the concentration $[MV^{2+}]$ = 0.1 mmol $L^{-1}$ in the final binary colloid. Table 1 summarizes the prepared binary colloids with their composition.

*2.3. Observations of photoinduced electron transfer and photocatalytic hydrogen*

*evolution*

We examined two photochemical reactions separately for the niobate–clay binary colloids. One was photoinduced electron transfer from niobate nanosheets to $MV^{2+}$ adsorbed on clay nanosheets, and the other was photocatalytic hydrogen evolution. The photochemical reactions examined for each sample were indicated in Table 1.

For the measurement of $MV^{2+}$ photoreduction [33], an aliquot (~ 5 mL) of a colloid sample was placed in a water-cooled (25 ºC) quartz cell (5 mm in thickness) capped with a rubber septum. After bubbling with water-saturated nitrogen gas for 30 min, the sample was irradiated by an Ushio SX-UI500XQ 500-W Xe lamp for 8 min. After the irradiation was stopped, the cell was stood with flowing $N_2$ in the headspace, and visible spectra of the samples were measured repeatedly. During the experiment, the cell was kept as static as possible. Visible absorption spectra were recorded on a Shimadzu UV-2600 spectrophotometer before and after the irradiation, and the amount of photogenerated methylviologen monoradical cations ($MV^{+\bullet}$) was determined from the characteristic absorption of the radical cations at 600 nm [42].

Photocatalytic hydrogen evolution was measured with a batch system [43]. A colloid sample (5 mL) was poured into a cylindrical quart test tube (20 mL). After nitrogen bubbling for 30 min, the tube was sealed with a rubber septum and irradiated by UV light using a Xe lamp (USHIO SX-U1500XQ) through a HOYA U330 filter to remove visible light. After the irradiation for 1 h, the amount of evolved hydrogen gas in the headspace was analyzed by an on-line gas chromatograph with a thermal conductivity detector (Agilent Technology Co. 490 MicroGC) equipped with an MS-5A column. The column temperature and the column pressure was fixed at 100 °C and 170 kPa, respectively. He gas was used as the carrier gas.

## 3. Results and discussion

### *3.1. Characterization of colloid samples*

According to the method of Varade and Haraguchi [41], Pt nanoparticles are successfully deposited on clay nanosheets. Heat treatment of a niobate–clay binary colloid after addition of $H_2PtCl_4$ turns the color of the sample to pale black, indicating deposition of metallic Pt on clay nanosheets (Fig. 2a). A TEM image of the solid particles recovered from the colloids shows deposition of Pt nanoparticles with diameter of around 10 nm (Fig. 2b). XPS spectrum exhibits Pt 4f peaks at 73.1 and 76.3 eV, supporting the formation of metallic Pt (Fig. 2c) [44].

All of the niobate–clay binary nanosheet colloids show a similar appearance characterized by macroscopic homogeneity, which is kept for at least a week. Naked-eye observations of the colloids in flat glass capillaries show apparent homogeneity for all of the samples (Fig. 3a). Also, observations between crossed polarizers exhibit birefringence for all of the samples, and the birefringent part is delocalized in whole part of each sample (Fig. 3b). Such sample appearances and stability are little affected by loading of $MV^{2+}$ cations and/or Pt nanoparticles on clay nanosheets. The apparent homogeneity of the samples is ascribed to the phase separation of niobate and clay nanosheets at a micrometer scale [31]. The birefringence is caused by the liquid crystalline ordering of niobate nanosheets and indicates homogeneous distribution of the liquid crystalline domains of niobate nanosheets spreading in whole of the sample.

### *3.2. Photoinduced electron transfer to electron acceptor molecules adsorbed on clay*

As described above, we have investigated two types of reactions:

photoreduction of $MV^{2+}$ adsorbed on clay nanosheets and photocatalytic hydrogen evolution from water in the niobate–clay binary nanosheet colloids. Both of the reactions are initiated by releasing conduction-band electrons from semiconducting niobate nanosheets upon photoexcitation by UV light, as illustrated in Fig. 1. For the former reaction, the released electrons come to clay nanosheets are captured by the adsorbed $MV^{2+}$ molecules and reduce them. $MV^{+\bullet}$ radical cations form as the product. For the latter reaction, the released electrons are transferred to the liquid phase. In both the cases, positive holes generated in the photocatalytic niobate nanosheets are oxidatively consumed by propylammonium ions present at the nanosheets. This species is introduced as the exfoliating reagent in preparation of niobate nanosheets to replace $K^+$ ions compensating negative charges of niobate $Nb_6O_{17}^{4-}$ layers, and stays on the exfoliated colloidal nanosheets as their countercations with the amount of 0.9 molecule per $Nb_6O_{17}^{4-}$ unit [45]. Oxidative decomposition of organoammonium cations adsorbed on niobate nanosheets by surface $OH^\bullet$ and $O_2^{\bullet-}$ species upon UV excitation on these photocatalytic nanosheets has already been reported by previous studies [46, 47].

The niobate–$MV^{2+}$/clay binary nanosheet colloid, where $MV^{2+}$ molecules are adsorbed on clay nanosheets as acceptors of electrons come from niobate nanosheets, undergoes photoinduced electron transfer upon UV irradiation [32, 33]. This is spectroscopically indicated by the formation $MV^{+\bullet}$ that is characterized by strong absorption bands at 400 and 600 nm [36] as shown in Fig. 4a. Photogenerated $MV^{+\bullet}$ species is stably kept in the colloid as indicated by its lifetime for several tens of minutes as indicated in Fig. 5 (entry 3). This is ascribed to the phase separation of niobate and clay nanosheets. This results in spatial separation of electron donors (niobate nanosheets) and acceptors ($MV^{2+}$ molecules on clay nanosheets) to keep the photoproduct

with suppression of the backward reactions.

In contrast, a niobate–$MV^{2+}$/Pt/clay binary colloid, where Pt nanoparticles are co-loaded with $MV^{2+}$ molecules on clay nanosheets, gives drastically decreased amount and stability of photogenerated $MV^{+\bullet}$ molecules compared to the niobate–$MV^{2+}$/clay colloid as shown in Fig. 4b. Their amount and lifetime are about 1/10 those generated in the sample lacking Pt nanoparticles as indicated in Fig. 5 (entry 5). Suppression of $MV^{+\bullet}$ generation is more pronounced for the Pt/niobate–$MV^{2+}$/clay colloid (entry 10) because $MV^{+\bullet}$ was not detected by UV-vis spectroscopy. These results indicate competitive generation of $MV^{+\bullet}$ and $H_2$ (via Pt) by the electrons transferred from niobate nanosheets to clay particles, as discussed later.

*3.3. Photocatalytic hydrogen evolution*

The hydrogen evolution from niobate–clay binary nanosheet colloids upon UV irradiation is ascribed to the photocatalytic reduction of $H^+$ in the aqueous medium of colloids. This reaction proceeds if conduction-band electrons generated in the photoexcited hexaniobate ($Nb_6O_{17}^{4-}$) nanosheets are released into water. We have already reported higher activity of niobate nanosheet than $TiO_2$ (P-25) for photocatalytic hydrogen evolution from water [22]. This is ascribed to the large surface of exfoliated niobate nanosheets; the surface area is calculated to be 353 $m^2\ g^{-1}$ (as $Nb_6O_{17}^{4-}$) for niobate nanosheets if $K_4Nb_6O_{17}$ crystals are ideally exfoliated to form bilayer nanosheets [45, 48]. The photocatalytic activity of niobate nanosheets is affected by mixing with clay nanosheets. All of the niobate–clay binary aqueous nanosheet colloids evolve hydrogen more or less upon UV irradiation. The role of clay nanosheets, whose surface area is 900 $m^2\ g^{-1}$ [49], varies with modification, i.e., the species loaded on them. Fig.

6 summarizes the results.

The amount of evolved hydrogen depends on the modification of clay nanosheets. Samples lacking Pt nanoparticles exhibit low activity for the hydrogen evolution (entries 1–3) because of the absence of cocatalytic Pt particles for efficient electron transfer to $H^+$ ions. Activity of the niobate-clay binary colloid without $MV^{2+}$ and Pt (entry 2) is similar to (or somewhat lower than) that of a single-component niobate colloid (entry 1) in the absence of Pt. This indicates that clay nanosheets coexisting with photocatalytic niobate nanosheets do not work as cocatalyst for hydrogen evolution because of the inertness of clay minerals (aluminosilicates) for electron transfer. Moreover, adsorption of $MV^{2+}$ on clay nanosheets in the absence of Pt cocatalyst does not improve the hydrogen evolution (entry 3).

Introduction of Pt cocatalyst to the niobate–clay binary nanosheet colloids greatly enhances photocatalytic hydrogen evolution activity (entries 4–10). Pt deposition onto photocatalytic niobate nanosheets is most effective (entry 8), and mixing with clay nanosheets reduces the activity (entries 9 and 10). However, mixture of niobate and Pt/clay nanosheets (entry 4) also shows the activity comparable to the Pt/niobate–clay colloid; the activity which is much higher than that of niobate–clay colloid (entry 2). In the niobate–Pt/clay sample, Pt nanoparticles are loaded on clay nanosheets, which are phase-separated from niobate nanosheets. This means spatial separation of the photocatalytic niobate nanosheets from the cocatalytic Pt-loaded clay nanosheets in time average in the colloid. The improved hydrogen evolution compared with the niobate–clay colloid indicates that the Pt nanoparticles on clay nanosheets work as the sites for transferring electrons from the photoexcited semiconductor nanosheets to aqueous protons to photocatalytically evolve hydrogen from water, even though the

cocatalyst is spatially separated from the photocatalytic nanosheets. The photochemical events observed for the niobate–$MV^{2+}$/clay and niobate–Pt/clay colloids demonstrate the role of clay nanosheets as turnout switches of electrons coming from photocatalytic niobate nanosheets. Destination of the electrons is determined by the species loaded on clay nanosheets.

*3.4. Hydrogen evolution with co-loading of Pt and $MV^{2+}$ on clay nanosheets*

UV irradiation of a niobate–Pt/$MV^{2+}$/clay binary nanosheet colloid, where Pt nanoparticles and $MV^{2+}$ molecules are co-loaded on clay nanosheets, generates both of $MV^{+\bullet}$ and $H_2$ species (Fig. 6, entry 5). However, the amount of $MV^{+\bullet}$ molecules are smaller by an order of magnitude than those observed for the niobate–$MV^{2+}$/clay colloid lacking Pt (Fig. 5, entry 3). In niobate–$MV^{2+}$/clay colloid, the absolute amount of photogenerated $MV^{+\bullet}$ is estimated as 0.12 μmol from the $MV^{+\bullet}$ concentration (Fig. 5) and colloid volume 5 mL, whereas that in the niobate–Pt/$MV^{2+}$/clay colloid is 0.015 μmol. Also, the amount of evolved hydrogen is also about 25% that obtained by the niobate–Pt/clay colloid without $MV^{2+}$. These results show competitive relationship of the two electron transfer pathways: reduction of adsorbed $MV^{2+}$ molecules and reduction of aqueous $H^+$ ions. Electrons come to clay nanosheets from photoexcited niobate nanosheets partly go to aqueous $H^+$ ions via Pt nanoparticles as well as adsorbed $MV^{2+}$ ions.

However, the $MV^{2+}$ reduction pathway does not simply suppress the hydrogen evolution pathway in the niobate–Pt/$MV^{2+}$/clay binary nanosheet colloid. Lager amounts of $MV^{2+}$ adsorbed on clay nanosheets increases the amount of evolved hydrogen as well as the amount of $MV^{+\bullet}$ (entries 5–7). This result is rationalized by the occurrence

of electron transfer from photogenerated $MV^{+\bullet}$ adsorbed on clay nanosheets to aqueous $H^+$ ions via coadsorbed Pt nanoparticles as a minor pathway of the hydrogen evolution. Because this stepwise hydrogen evolution is less efficient than the direct electron transfer that skips the $MV^{+\bullet}/MV^{2+}$ redox cycle, the coadsorption of $MV^{2+}$ with Pt nanoparticles totally reduces the activity of the niobate–clay nanosheet colloids for photocatalytic hydrogen evolution.

The lifetimes of $MV^{+\bullet}$ also agree with this assumption. The fast $MV^{+\bullet}$ decay observed for the niobate–Pt/$MV^{2+}$/clay samples (entries 5–7) can be rationalized by consumption of electrons on $MV^{+\bullet}$ for the reduction of $H^+$. The $MV^{+\bullet}$ lifetime of synchronously changes with its amount, suggesting slow electron transfer from adsorbed $MV^{+\bullet}$ to aqueous $H^+$; however, more detailed quantitative analyses including time-lapse measurements and estimation of the amount of photogenerated electrons and holes are necessary in the future.

*3.5. Effect of stirring on the hydrogen evolution*

Whereas the above results were all obtained under static conditions without stirring the colloid samples, the photocatalytic hydrogen evolution of niobate–Pt/clay and niobate–Pt/$MV^{2+}$/clay binary nanosheet colloids was also affected by stirring the sample during the UV irradiation. The stirring was carried out by using a Teflon-coated magnetic stirring bar. Amounts of hydrogen evolved from the stirred samples are also shown in Fig. 6 (entries 4b and 5b). The photocatalytic hydrogen evolution from the niobate–clay binary colloids is reduced by stirring the samples. For the niobate–Pt/clay colloid, the amount of evolved hydrogen with the sample stirring is less than a half that without stirring. Also, for the niobate–Pt/$MV^{2+}$/clay colloid, the amount from the stirred

sample is about 80% that from the static sample.

The negative impact of stirring would be related to the phase-separated structure of niobate–clay binary colloids. As described above, the phase separation causes spatial separation of the photocatalytic niobate and cocatalytic clay nanosheets in colloids. Stirring of the samples facilitates contact of both the nanosheets, and also that between nanosheets and aqueous $H^+$ ions. However, our results indicate that such contact reduces the efficiency of electron transfer from photocatalytic niobate nanosheets to $H^+$ ions via Pt cocatalyst on clay nanosheets. The spatial separation between niobate and clay nanosheets, which the structure is broken by stirring the colloids, would be a key to the efficient electron transfer. We have already found that $MV^{+\bullet}$ ions photogenerated in niobate–clay binary nanosheet colloid is greatly destabilized by stirring the colloid [32], which is ascribable to failure in the separation of electron donor (niobate nanosheets) and acceptor ($MV^{2+}$ molecules on clay nanosheets) for suppressing the backward reaction in the stirred colloid. This would also be the case for the electron transfer originated from niobate nanosheets and destined for aqueous $H^+$ ions via Pt nanoparticles on clay nanosheets in the present study. Heterogeneous photocatalytic reactions are generally carried out under stirred conditions in order to facilitate contact of photocatalyst particles and dissolved reactants. However, our findings indicate importance of the colloidal structure of photocatalytic and cocatalytic particles; optimum structures are not always provided by intimate mixing of the particles by simply stirring the colloidal reaction systems.

## 4. Conclusions

Photochemical processes in the niobate–clay aqueous binary colloids are

initiated by photoexcitation of photocatalytic niobate nanosheets, and successive electron transfer in the dark is controlled by optically and electrically inert clay nanosheets. Destination of the electrons traveled from niobate nanosheets is determined by the species loaded on clay nanosheets. $MV^{2+}$ molecules adsorbed on clay nanosheets accept the electrons to form $MV^{+\bullet}$, by which electrons are trapped at clay nanosheets. However, when Pt nanoparticles are loaded on clay nanosheets, the electrons are transferred to the solution phase and reduce $H^+$ ions to evolve hydrogen gas from the colloid. Although $MV^{2+}$ and Pt are basically in competition for the electron transfer in the case of co-loading, electrons captured by $MV^{2+}$ (as the formation of $MV^{+\bullet}$) are partly transferred to aqueous $H^+$ to contribute to the hydrogen evolution as a minor pathway. The negative effect of sample stirring on the hydrogen evolution demonstrates the contribution of spatial separation of photocatalytic niobate and cocatalytic clay nanosheets at a micrometer level. These results indicate that transfer routes and destinations of electrons released from the same semiconductor photocatalyst can be controlled in the dark by independent additives such as clay particles coexisting in the reaction system. Also, the total process is affected by the colloidal structure of dispersed particles. These will lead to development of more precise design of photocatalytic reaction systems from the same photocatalyst.

**Acknowledgment**

This work was partly supported by a JSPS KAKENHI (No. 16K14095 for T. N.) and ACT-C (Grant Number JPMJCR12Y5 for T. O.). Financial support by Initiative for Realizing Diversity in the Research Environment, MEXT, Japan (for E. M.) was also acknowledged. We thank Jie Zhang and Tomoaki Tanaka for their assistance with the TEM and XPS analyses, respectively.

**References**

[1] M.A. Fox, M.T. Dulay, Chem. Rev., 93 (1993) 341-357.

[2] V. Ramamurthy, K.S. Schanze, Solid State and Surface Photochemistry, Molecular and Supramolecular Photochemistry, Marcel Dekker, New York, 2000.

[3] V. Ramamurthy, K.S. Schanze, Semiconductor photochemistry and photophysics, Molecular and Supramolecular Photochemistry, Marcel Dekker, New York, 2003.

[4] F.E. Osterloh, Chem. Mater., 20 (2008) 35-54.

[5] S. Sato, J.M. White, J. Phys. Chem., 85 (1981) 592-594.

[6] K. Maeda, K. Domen, Bull. Chem. Soc. Jpn., 89 (2016) 627-648.

[7] H. Tsukahara, Bull. Soc. Sci. Photogr. Jpn., 1969 (1969) 11-21.

[8] E. Borgarello, J. Kiwi, E. Pelizzetti, M. Visca, M. Graetzel, J. Am. Chem. Soc., 103 (1981) 6324-6329.

[9] Y. Tian, T. Tatsuma, J. Am. Chem. Soc., 127 (2005) 7632-7637.

[10] J. Ran, M. Jaroniec, S.Z. Qiao, Adv. Mater., 30 (2018) 1704649.

[11] K. Maeda, ACS Catal., 3 (2013) 1486-1503.

[12] T. Ohno, K. Tokieda, S. Higashida, M. Matsumura, Appl. Catal. A, 244 (2003) 383-391.

[13] K. Hirano, K. Inoue, T. Yatsu, J. Photochem. Photobiol. A, 64 (1992) 255-258.

[14] K. Sayama, K. Mukasa, R. Abe, Y. Abe, H. Arakawa, Chem. Commun., (2001) 2416-2417.

[15] C.-y. Wang, C. Böttcher, D.W. Bahnemann, J.K. Dohrmann, J. Mater. Chem., 13 (2003) 2322-2329.

[16] H. Zhang, G. Chen, D.W. Bahnemann, J. Mater. Chem., 19 (2009) 5089.

[17] C.-T. Dinh, M.-H. Pham, F. Kleitz, T.-O. Do, J. Mater. Chem. A, 1 (2013) 13308-13313.

[18] Y. Ide, M. Matsuoka, M. Ogawa, ChemCatChem, 4 (2012) 628-630.

[19] Y. Ide, M. Torii, T. Sano, J. Am. Chem. Soc., 135 (2013) 11784-11786.

[20] Y. Ide, N. Kagawa, M. Sadakane, T. Sano, Chem. Commun., 49 (2013) 9027-9029.

[21] M. Ogawa, M. Sohmiya, Y. Watase, Chem. Commun., 47 (2011) 8602-8604.

[22] T. Nakato, T. Fujita, E. Mouri, Phys. Chem. Chem. Phys., 17 (2015) 5547-5550.

[23] K. Domen, A. Kudo, A. Shinozaki, A. Tanaka, K. Maruya, T. Onishi, J. Chem. Soc., Chem. Commun., (1986) 356-357.

[24] A. Kudo, A. Tanaka, K. Domen, K. Maruya, K. Aika, T. Onishi, J. Catal., 111 (1988) 67-76.

[25] J.H. Alstrum-Acevedo, M.K. Brennaman, T.J. Meyer, Inorg. Chem., 44 (2005) 6802-6827.

[26] J. Barber, Chem. Soc. Rev., 38 (2009) 185-196.

[27] T. Nakato, N. Miyamoto, Materials, 2 (2009) 1734-1761.

[28] T. Nakato, N. Miyamoto, J. Mater. Chem., 12 (2002) 1245-1246.

[29] H. van Olphen, Clay colloid chemistry (reprinted edition), Krieger, Malabar, 1991.

[30] T. Nakato, J. Kawamata, S. Takagi, Inorganic nanosheets and nanosheet-based materials, Springer, Tokyo, 2017.

[31] N. Miyamoto, T. Nakato, Langmuir, 19 (2003) 8057-8064.

[32] N. Miyamoto, Y. Yamada, S. Koizumi, T. Nakato, Angew. Chem. Int. Ed., 46 (2007) 4123-4127.

[33] T. Nakato, Y. Yamada, N. Miyamoto, J. Phys. Chem. B, 113 (2009) 1323-1331.

[34] T. Nakato, Y. Yamada, M. Nakamura, A. Takahashi, J. Colloid Interface Sci., 354

(2011) 38-44.

[35] T. Nakato, S. Inoue, Y. Hiraragi, J. Sugawara, E. Mouri, H. Aritani, J. Mater. Sci., 49 (2014) 915-922.

[36] P.M.S. Monk, The Viologens, John Wiley & Sons, Chichester, 1998.

[37] N. Miyamoto, H. Yamamoto, R. Kaito, K. Kuroda, Chem. Commun., (2002) 2378-2379.

[38] N. Miyamoto, T. Nakato, J. Phys. Chem. B, 108 (2004) 6152-6159.

[39] K. Nassau, J.W. Shiever, J.L. Bernstein, J. Electrochem. Soc., 116 (1969) 348-353.

[40] P. Levitz, E. Lecolier, A. Mourchid, A. Delville, S. Lyonnard, Europhys. Lett., 49 (2000) 672-677.

[41] D. Varade, K. Haraguchi, Langmuir, 29 (2013) 1977-1984.

[42] T. Watanabe, K. Honda, J. Phys. Chem., 86 (1982) 2617-2619.

[43] S. Kamimura, S. Abe, T. Tsubota, T. Ohno, J. Photochem. Photobiol. A, 356 (2018) 263-271.

[44] T.A. Ivandini, R. Sato, Y. Makide, A. Fujishima, Y. Einaga, Diamond Relat. Mater., 14 (2005) 2133-2138.

[45] T. Nakato, N. Miyamoto, A. Harada, H. Ushiki, Langmuir, 19 (2003) 3157-3163.

[46] Y. Umemura, E. Shinohara, A. Koura, T. Nishioka, T. Sasaki, Langmuir, 22 (2006) 3870-3877.

[47] M.C. Sarahan, E.C. Carroll, M. Allen, D.S. Larsen, N.D. Browning, F.E. Osterloh, J. Solid State Chem., 181 (2008) 1678-1683.

[48] G.B. Saupe, C.C. Waraksa, H.-N. Kim, Y.J. Han, D.M. Kaschak, D.M. Skinner, T.E. Mallouk, Chem. Mater., 12 (2000) 1556-1562.

[49] Technical Information B-RI 21 about Laponite provided by BYK Additives &

Instruments.

Table

Table 1. Composition of the prepared niobate–clay binary nanosheet colloid samples and photochemical reactions examined for each sample.

| Entry | Sample | Composition | | | | Photochemical reactions[a] | |
|---|---|---|---|---|---|---|---|
| | | Niobate g $L^{-1}$ | Clay g $L^{-1}$ | $MV^{2+}$ mmol $L^{-1}$ | Pt mass% | $MV^{2+}$ reduction | Hydrogen evolution |
| 1 | Niobate | 1 | 0 | 0 | 0 | – | + |
| 2 | Niobate–clay | 1 | 5 | 0 | 0 | – | + |
| 3 | Niobate–$MV^{2+}$/clay | 1 | 5 | 0.1 | 0 | + | + |
| 4 | Niobate–Pt/clay | 1 | 5 | 0 | 0.5[b] | – | + |
| 4b | Niobate–Pt/clay | 1 | 5 | 0 | 0.5[b] | – | +[d] |
| 5 | Niobate–Pt/$MV^{2+}$/clay | 1 | 5 | 0.1 | 0.5[b] | + | + |
| 5b | Niobate–Pt/$MV^{2+}$/clay | 1 | 5 | 0.1 | 0.5[b] | – | +[d] |
| 6 | Niobate–Pt/$MV^{2+}$/clay | 1 | 5 | 0.05 | 0.5[b] | + | + |
| 7 | Niobate–Pt/$MV^{2+}$/clay | 1 | 5 | 0.15 | 0.5[b] | + | + |
| 8 | Pt/niobate | 1 | 0 | 0 | 0.5[c] | – | + |
| 9 | Pt/niobate–clay | 1 | 5 | 0 | 0.5[c] | – | + |
| 10 | Pt/niobate– $MV^{2+}$/clay | 1 | 5 | 0.1 | 0.5[c] | + | + |

[a] Examined: +, not examined: –.

[b] Mass% with respect to the mass of clay.

[c] Mass% with respect to the mass of niobate (as $Nb_6O_{17}^{4-}$).

[d] Carried out under a stirred condition.

Figure captions

Fig. 1. Schematic representation of the structure and photocatalytic reactions in the niobate–clay binary nanosheet system.

Fig. 2. (a) Photograph of clay (left) and Pt/clay nanosheet (right) colloids ([clay] = 10 g $L^{-1}$, Pt 0.5 wt%), (b) TEM image and (c) XPS spectrum of Pt/clay nanosheets obtained from the Pt/clay nanosheet colloid shown in (a).

Fig. 3. Appearances of (a) niobate–clay (b) niobate–$MV^{2+}$/clay (c) niobate–Pt/clay (d) niobate–Pt/$MV^{2+}$/clay colloids without (above) and with (below) crossed polarizers (([niobate] = 5 g $L^{-1}$, [clay] = 10 g $L^{-1}$, Pt 0.1 wt%)).

Fig. 4. Visible absorption spectra of (a) niobate–Pt/$MV^{2+}$/clay and (b) niobate–$MV^{2+}$/clay colloids before and after UV irradiation for 8 min.

Fig. 5. Photoinduced electron transfer in various niobate–clay binary colloid samples involving $MV^{2+}$ species measured by the concentration and lifetime of photogenerated $MV^{+\bullet}$ species.

Fig. 6. Photocatalytic activities of various niobate–clay binary colloid samples for hydrogen evolution from water compared by the amount of hydrogen evolved for UV irradiation for 60 min.

Fig. 1

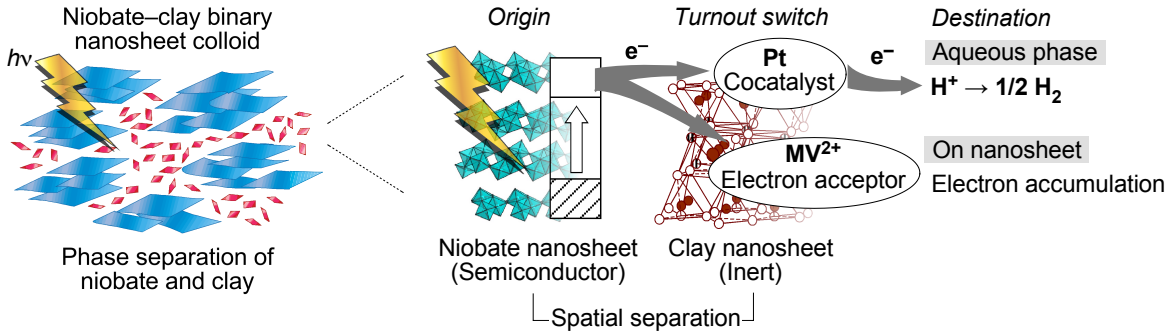


Fig. 1. Schematic representation of the structure and photocatalytic reactions in the niobate–clay binary nanosheet system.

Fig. 2

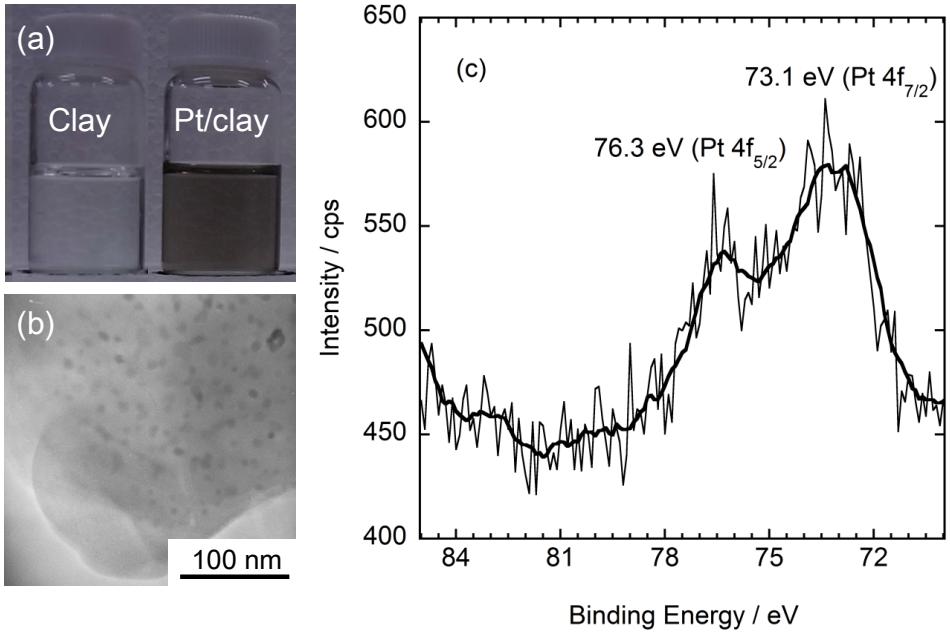


Fig. 2. (a) Photograph of clay (left) and Pt/clay nanosheet (right) colloids ([clay] = 10 g $L^{-1}$, Pt 0.5 wt%), (b) TEM image and (c) XPS spectrum of Pt/clay nanosheets obtained from the Pt/clay nanosheet colloid shown in (a).

Fig. 3

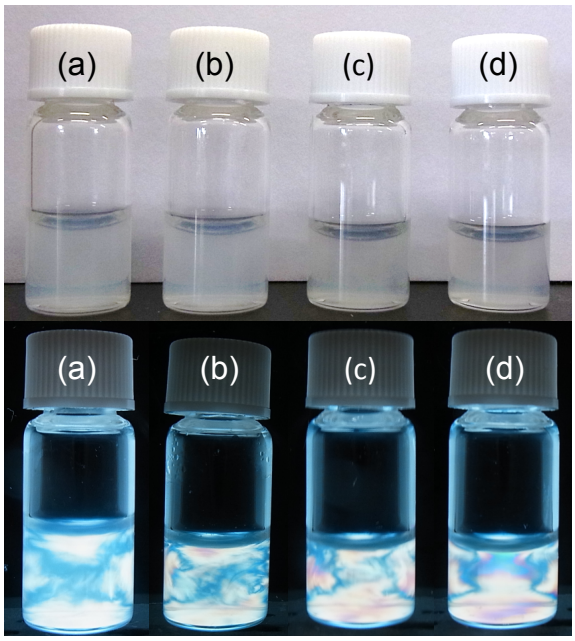


Fig. 3. Appearances of (a) niobate–clay (b) niobate–$MV^{2+}$/clay (c) niobate–Pt/clay (d) niobate–Pt/$MV^{2+}$/clay colloids without (above) and with (below) crossed polarizers (([niobate] = 5 g $L^{-1}$, [clay] = 10 g $L^{-1}$, Pt 0.1 wt%)).

Fig. 4

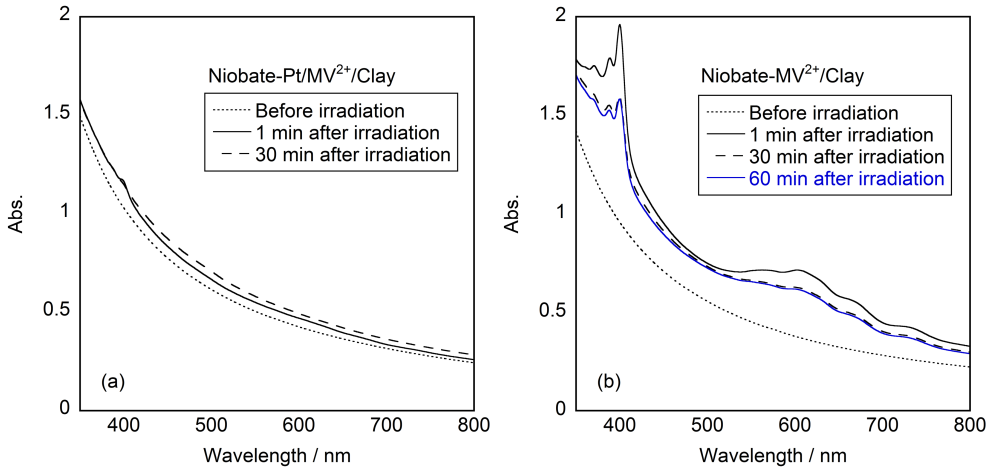


Fig. 4. Visible absorption spectra of (a) niobate–Pt/$MV^{2+}$/clay and (b) niobate–$MV^{2+}$/clay colloids before and after UV irradiation for 8 min.

Fig. 5

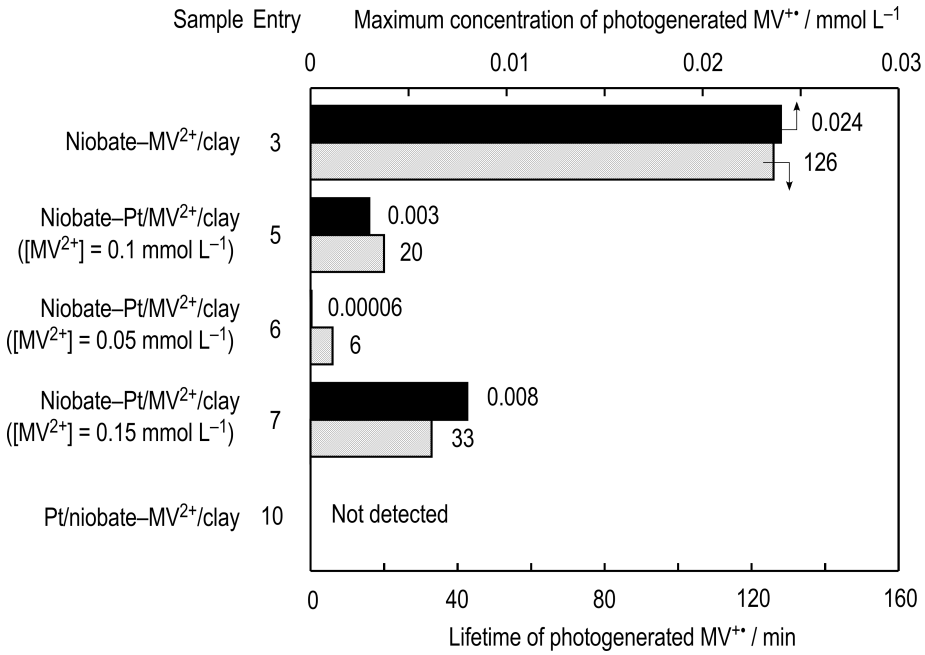


Fig. 5. Photoinduced electron transfer in various niobate–clay binary colloid samples involving $MV^{2+}$ species measured by the concentration and lifetime of photogenerated $MV^{+\bullet}$ species.

Fig. 6

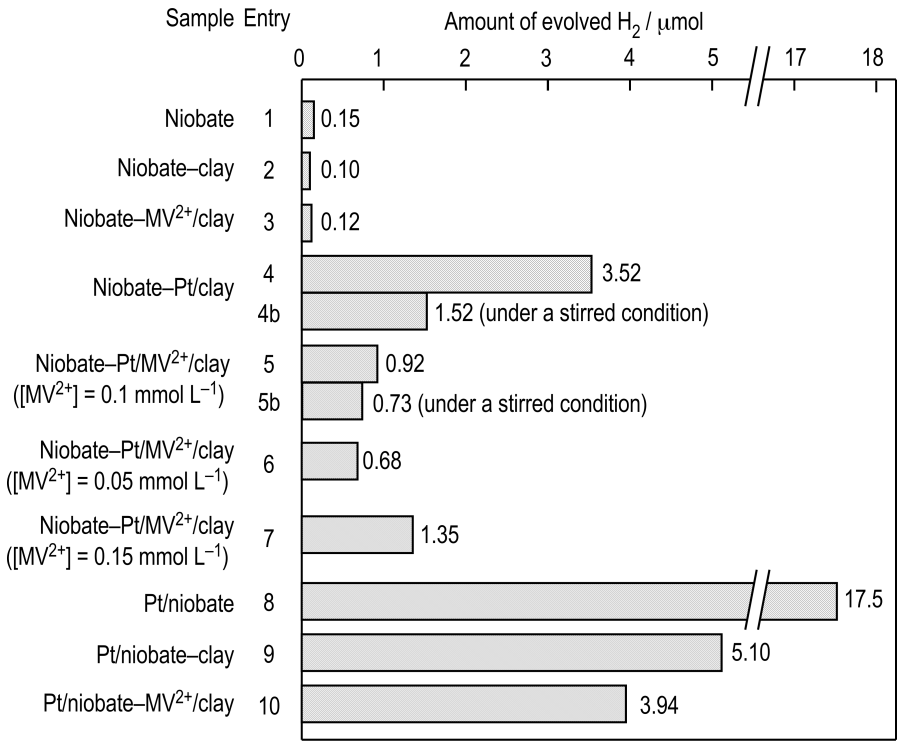


Fig. 6. Photocatalytic activities of various niobate–clay binary colloid samples for hydrogen evolution from water compared by the amount of hydrogen evolved for UV irradiation for 60 min.